PNAS RESEARCH ARTICLE | MICROBIOLOGY OPEN ACCESS

A next-generation intranasal trivalent MMS vaccine induces durable and broad protection against SARS-CoV-2 variants of concern

Jiayu Xu[a,1], Yuexiu Zhang[a,1], Panke Qu[a,2], Mohamed M. Shamseldin[b,c,2], Sung J. Yoo[a,2], Jack Misny[d,2], Ilada Thongpan[d], Mahesh KC[d], Jesse M. Hall[b], John P. Evans[a], Mostafa Eltobgy[b], Mijia Lu[a], Chengjin Ye[e], Michelle Chamblee[a], Xueya Liang[a], Luis Martinez-Sobrido[e], Amal O. Amer[b,f], Jacob S. Yount[b,f], Prosper N. Boyaka[a,f], Mark E. Peeples[d,f,g], Shan-Lu Liu[a,b,f,h], Purnima Dubey[b,f], and Jianrong Li[a,f,3]

Edited by Peter Palese, Icahn School of Medicine at Mount Sinai, New York, NY; received November 30, 2022; accepted July 24, 2023

As SARS-CoV-2 variants of concern (VoCs) that evade immunity continue to emerge, next-generation adaptable COVID-19 vaccines which protect the respiratory tract and provide broader, more effective, and durable protection are urgently needed. Here, we have developed one such approach, a highly efficacious, intranasally delivered, trivalent measles-mumps-SARS-CoV-2 spike (S) protein (MMS) vaccine candidate that induces robust systemic and mucosal immunity with broad protection. This vaccine candidate is based on three components of the MMR vaccine, a measles virus Edmonston and the two mumps virus strains [Jeryl Lynn 1 (JL1) and JL2] that are known to provide safe, effective, and long-lasting protective immunity. The six proline-stabilized prefusion S protein (preS-6P) genes for ancestral SARS-CoV-2 WA1 and two important SARS-CoV-2 VoCs (Delta and Omicron BA.1) were each inserted into one of these three viruses which were then combined into a trivalent "MMS" candidate vaccine. Intranasal immunization of MMS in IFNAR1$^{-/-}$ mice induced a strong SARS-CoV-2-specific serum IgG response, cross-variant neutralizing antibodies, mucosal IgA, and systemic and tissue-resident T cells. Immunization of golden Syrian hamsters with MMS vaccine induced similarly high levels of antibodies that efficiently neutralized SARS-CoV-2 VoCs and provided broad and complete protection against challenge with any of these VoCs. This MMS vaccine is an efficacious, broadly protective next-generation COVID-19 vaccine candidate, which is readily adaptable to new variants, built on a platform with a 50-y safety record that also protects against measles and mumps.

SARS-CoV-2 | intranasal trivalent vaccine | MMR vaccine

The coronavirus disease 2019 (COVID-19) pandemic, caused by severe acute respiratory syndrome coronavirus 2 (SARS-CoV-2), has resulted in tremendous morbidity and mortality worldwide and continues to threaten all aspects of our society (1, 2). As of May 2, 2023, more than 6.9 million deaths and 764 million infected cases have been documented. Several types of SARS-CoV-2 vaccines have been approved for use in humans, including messenger RNA (mRNA), adenovirus-vectored, and subunit vaccines (3). Most of them use the prefusion spike (S) protein stabilized by two prolines (preS-2P) as the immunogen (4–6). Following two intramuscular injections, these vaccines are successful in preventing severe disease and death (4–6).

The continuous emergence of new SARS-CoV-2 variants of concern (VoCs) has made this pandemic difficult to halt. Since the pandemic began, several VoCs including the Alpha (B.1.1.7), Beta (B.1.351), Gamma (P.1), Delta (B.1.617.2), and, more recently, the dominant Omicron (B.1.1.529/BA.1) and its subvariants (BA.2, BA.2.12.1, BA.4, BA.5, and XBB.1.5) have emerged (7, 8). The Omicron BA.1 variant was first detected in South Africa in November 2021 and spread globally (9). Compared to earlier variants, the Omicron BA.1 S protein harbors the highest number of mutations in the receptor-binding domain (RBD), markedly reducing its sensitivity to neutralizing antibodies (NAbs) induced by the current COVID-19 vaccines (10).

Despite the high success of the current COVID-19 vaccines, there are several limitations, including their reduced effectiveness against SARS-CoV-2 VoCs, short duration of protection, inability to induce a mucosal immune response to protect the airways, and high cost of production or distribution (11, 12). Therefore, there is an urgent need to develop the next generation of intranasal COVID-19 vaccines which induce durable and broadly protective immunity, both in the airways and systemically.

The combined MMR (measles/mumps/rubella) vaccine has been available in the United States since 1971 and is one of the safest and most effective human vaccines (13, 14). The MMR vaccine contains attenuated strains of measles virus (MeV), mumps virus (MuV),

Significance

There is an urgent need to develop a mucosal SARS-CoV-2 vaccine that can induce broad, durable protection. MMR has been one of the safest and most successful vaccines in human history. By expressing the six-proline-stabilized prefusion spikes from three diverse SARS-CoV-2 strains in the MeV, MuV-JL1, and MuV-JL2 vaccine strains from MMR, we generated a MMS trivalent vaccine candidate. Intranasally delivered MMS induced strong SARS-CoV-2-specific neutralizing antibody, mucosal IgA, and systemic and lung resident T cell immune responses that provide broad protection against challenge with each of these three strains. Therefore, MMS is a highly promising next-generation vaccine candidate against COVID-19. Furthermore, any of the three component vaccine viruses can be quickly modified when a new important SARS-CoV-2 variant appears.

Competing interest statement: The Ohio State University Research Foundation has filed a patent application for the measles virus-based SARS-CoV-2 vaccine candidates. In addition, The Ohio State University Research Foundation and Abigail Wexner Research Institute at Nationwide Children's Hospital have filed a patent application for the mumps virus–based SARS-CoV-2 vaccine candidates.

This article is a PNAS Direct Submission.

[1]J.X. and Y.Z. contributed equally to this work.

[2]P.Q., M.M.S., S.J.Y., and J.M. contributed equally to this work.

[3]To whom correspondence may be addressed. Email: li.926@osu.edu.

This article contains supporting information online at https://www.pnas.org/lookup/suppl/doi:10.1073/pnas.2220403120/-/DCSupplemental.

Published October 5, 2023.

and rubella virus and confers lifelong protection against these three viruses (13). Both MeV and MuV are nonsegmented negative-sense RNA viruses belonging to the family *Paramyxoviridae*. Both MeV and MuV have been used as delivery platforms for experimental vaccines against highly pathogenic viruses (15–18).

Sequence analysis of the MuV Jeryl Lynn (JL) strain in the MMR vaccine has revealed two MuV substrains with substantially different nucleotide sequences, the major (JL1) component and the minor (JL2) component (19). Therefore, each of the three viruses (MeV, MuV-JL1, and MuV-JL2) in the MMR vaccine could be modified to express a different antigen as components of a trivalent vaccine candidate. This multivalent vaccine platform is highly attractive for the development of a next-generation SARS-CoV-2 vaccine because three S protein genes from different VoCs can be inserted into these three viruses, thereby providing broad protection against multiple SARS-CoV-2 VoCs. In addition, both MeV and MuV can be delivered by the intranasal route to induce mucosal immunity.

In this study, we have demonstrated the success in modifying the MMR vaccine to develop an intranasal, trivalent measles-mumps-SARS-CoV-2 (MMS) vaccine candidate harboring three stabilized prefusion spike with six prolines (preS-6P) from three different SARS-CoV-2 strains.

Results

Recovery and Characterization of rMuV-JL1 Expressing a Six Proline-Stabilized Prefusion Spike of SARS-CoV-2 Delta Variant. We recently showed that preS stabilized by 6 prolines (preS-6P) (20) induced six to eight times higher NAbs than preS-2P (21) in MuV-JL2 (18) and MeV (22) vectors. Therefore, we inserted a codon-optimized preS-6P gene of the Delta variant into the P–M gene junction of the MuV-JL1 genome (Fig. 1*A*). The resultant rMuV-JL1-Delta-preS-6P formed significantly smaller plaques (Fig. 1*B*) and showed delayed cytopathic effects (CPE) (Fig. 1*C*) and replication kinetics (Fig. 1*D*), compared to the parental rMuV-JL1 but reached similar titers (10^7 PFU/mL) in Vero CCL81 cells by 96 h postinoculation. Next, we characterized the expression of Delta preS-6P by MuV-JL1. rMuV-JL2 and rMuV-JL2-WA1-preS-6P were used as side-by-side controls. A strong preS-6P band was detected in the cell lysates and supernatants of both the rMuV-JL1-Delta-preS-6P (Fig. 1 *E*, *Left*) and the rMuV-JL2-WA1-preS-6P-infected cells (Fig. 1 *E*, *Right*), demonstrating that both the Delta and WA1 preS-6P were highly expressed and secreted by MuV-JL1 and MuV-JL2.

Recovery and Characterization of rMeV Expressing a Six Proline-Stabilized Prefusion Spike of SARS-CoV-2 Omicron BA.1. We inserted the codon-optimized preS-6P version of the Omicron BA.1 gene into the P–M gene junction of the MeV Edmonston vaccine strain genome to produce rMeV-BA.1-preS-6P (Fig. 2*A*). rMeV-BA.1-preS-6P formed smaller plaques (Fig. 2*B*) and showed delayed CPE (Fig. 2*C*) and replication (Fig. 2*D*) in Vero CCL81 cells compared to the parental rMeV. A strong preS-6P protein band was detected in both cell lysate and supernatant in rMeV-BA.1-preS-6P-infected cells (Fig. 2*E*), demonstrating that the Omicron BA.1 preS-6P is highly expressed by the MeV vector.

Trivalent Vaccine Induces a Broader Neutralizing Antibody Response than the Monovalent Vaccine in IFNAR1$^{-/-}$ Mice. Having thoroughly characterized all recombinant viruses, we next combined equal amounts (PFU) of rMeV-BA.1-preS-6P, rMuV-JL1-Delta-preS-6P, and rMuV-JL2-WA1-preS-6P to generate a trivalent MMS vaccine candidate. As a vector control, we combined equal amounts (PFU) of rMeV, rMuV-JL1, and rMuV-JL2 (MMM vector control). Then, we tested the immunogenicity of the trivalent MMS vaccine

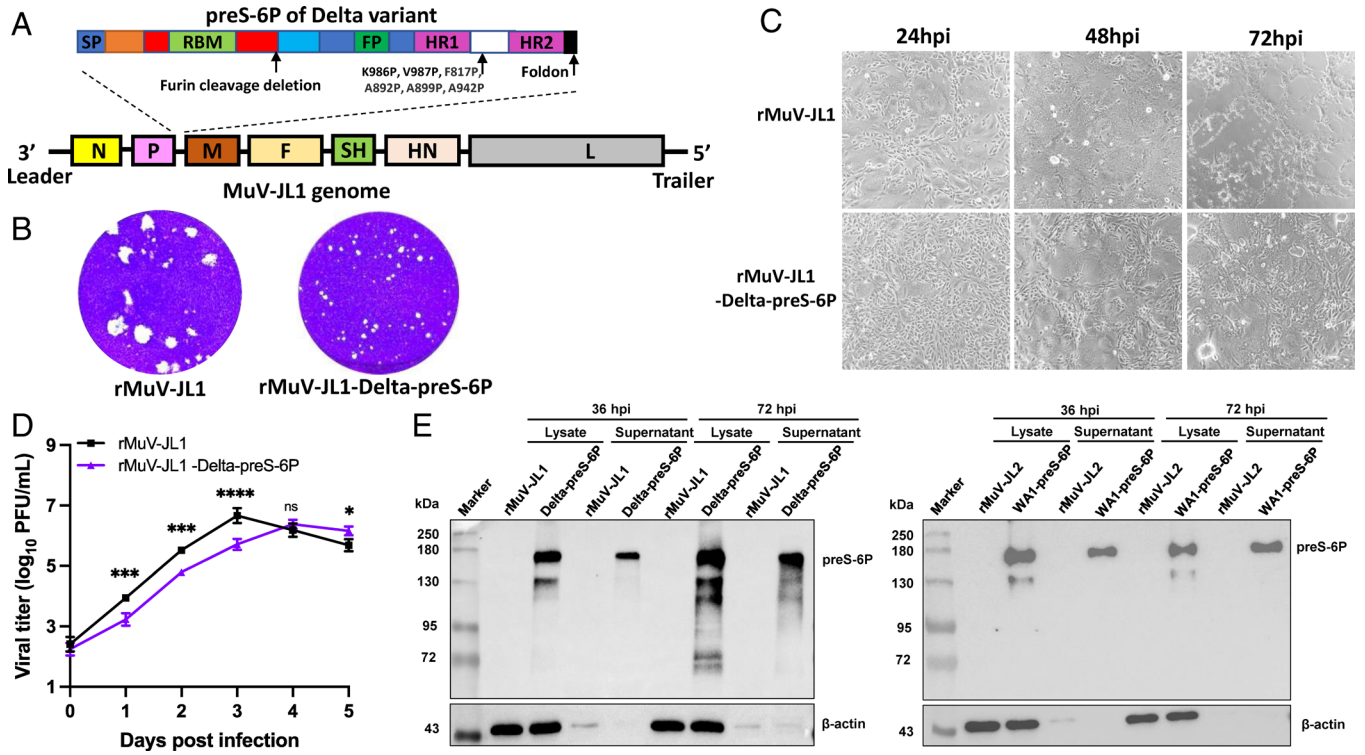

Fig. 1. Recovery and characterization of rMuV-JL1-Delta-preS-6P expressing the six proline-stabilized prefusion spike of SARS-CoV-2 Delta variant. (*A*) Strategy for insertion of preS-6P of the Delta variant into the P and M gene junction in the MuV-JL1 genome. (*B*) The plaque morphology of rMuV-JL1 and rMuV-JL1-Delta-preS-6P in Vero CCL81 cells at day 5. (*C*) rMuV-JL1-Delta-preS-6P exhibits delayed syncytia formation in Vero CCL81 cells (MOI of 0.1). (*D*) Replication kinetics of recombinant viruses in Vero CCL81 cells at an MOI of 0.1. (*E*) Expression of preS-6P in rMuV-JL1-Delta-preS-6P (*Left*) or rMuV-JL2-WA1-preS-6P (*Right*)-infected Vero CCL81 cells. An MOI of 0.1 was used for infection, and 10 μL of cell lysate (from total 200 μL) and 10 μL (from total 1 mL) of supernatant were used for Western blot.

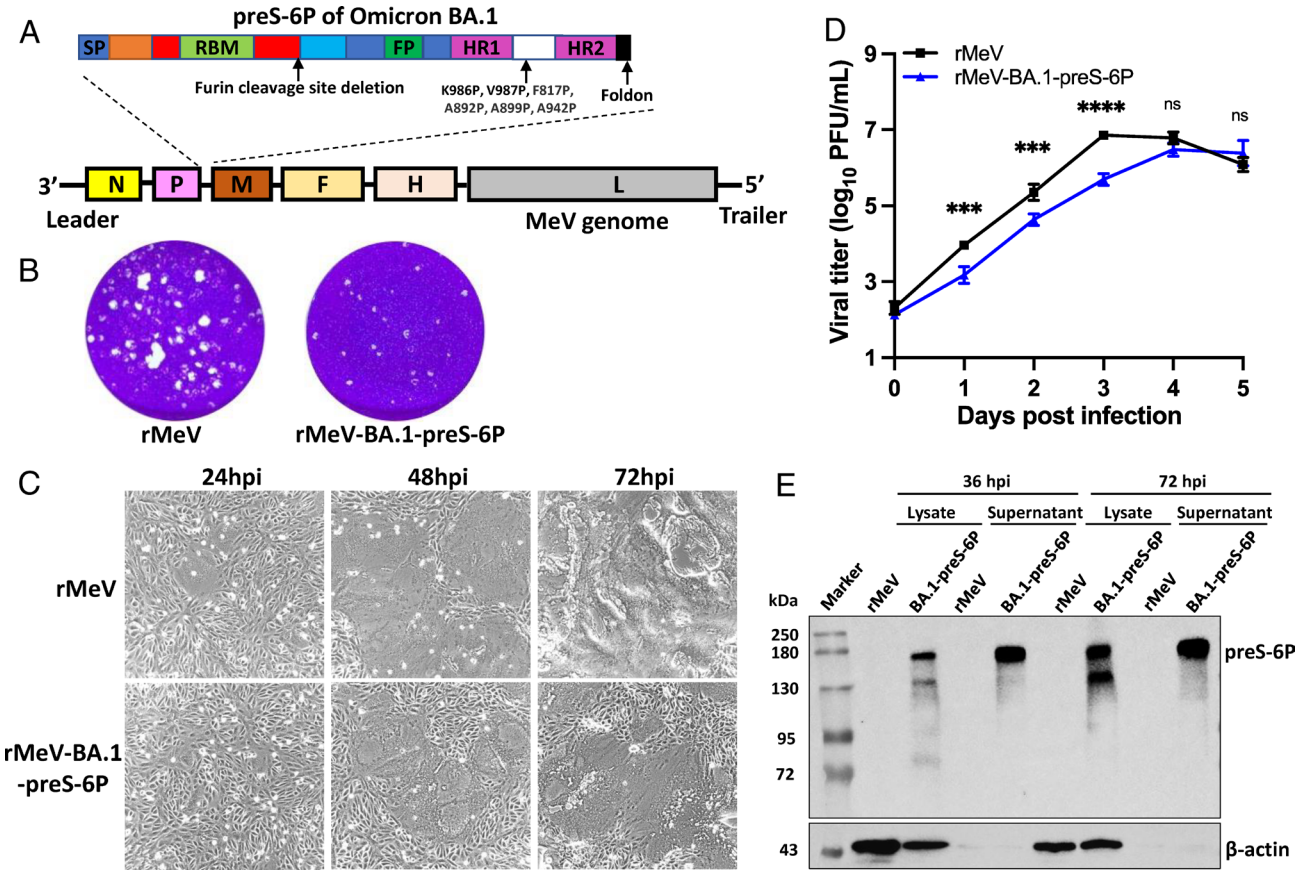

Fig. 2. Recovery and characterization of rMeV-BA.1-preS-6P expressing the six proline-stabilized prefusion spike of SARS-CoV-2 BA.1. (*A*) Strategy for insertion of preS-6P of Omicron BA.1 into the P and M gene junction in the MeV genome. (*B*) The plaque morphology of rMeV-preS-BA.1 in Vero CCL81 cells at day 5. (*C*) rMeV-BA.1-preS-6P exhibits delayed syncytia formation in Vero CCL81 cells (MOI of 0.1). (*D*) Replication kinetics of recombinant viruses in Vero CCL81 cells at an MOI of 0.1. (*E*) Expression of preS-6P of Omicron BA.1 by the MeV vector in Vero CCL81 cells. An MOI of 0.1 was used for infection, and 10 μL of cell lysate (from total 200 μL) and 10 μL (from total 1 mL) of supernatant were used for Western blot.

candidate in IFNAR1$^{-/-}$ mice, which are susceptible to infection by MeV, MuV, and mouse-adapted (MA) SARS-CoV-2 (17, 18). A monovalent vaccine candidate, rMeV-BA.1-preS-6P, was used for side-by-side comparison. Briefly, IFNAR1$^{-/-}$ mice were immunized with either a low dose (total of 5×10^5 PFU; 1.67×10^5 PFU of each of the three viruses) or a high dose (total of 1.5×10^6 PFU; 5.0×10^5 PFU of each virus) of each vaccine via combination of subcutaneous (*s.c.*) and intranasal (*i.n.*) routes and were boosted 3 wk later (Fig. 3*A*).

To detect SARS-CoV-2 S-specific IgG and IgA antibody titers, purified preS-6P proteins (*SI Appendix*, Fig.S1) of WA1, Delta, and Omicron BA.1 were used for ELISA. For the high-dose immunization groups, high levels of SARS-CoV-2 WA1 S-specific IgG (Fig. 3*B*), Delta S-specific IgG (Fig. 3*C*), and BA.1 S-specific IgG (Fig. 3*D*) were detected in both the monovalent and trivalent vaccine groups. WA1 S-specific IgG (Fig. 3*B*) and Delta S-specific IgG (Fig. 3*C*) in the trivalent vaccine were higher than that in the monovalent vaccine, but only the week 2 sera were significantly different. Similarly, BA.1 S-specific antibody in the trivalent vaccine group was higher than in the monovalent vaccine group, but there was no significant difference (Fig. 3*D*). Importantly, WA1, Delta, and BA.1 S-specific IgA titers were significantly higher in the trivalent vaccine group than those in the monovalent vaccine group (Fig. 3 *E*–*G*). In addition, WA1 and BA.1 S-specific IgA titers were higher than Delta S-specific IgA titers (Fig. 3 *E*–*G*).

Next, sera from week 7 were used to quantify the serum NAbs against SARS-CoV-2 D614G, Delta, Omicron BA.1, and BA.4/5 using a pseudotyped lentivirus neutralization assay (23) (Fig. 3*H*). As expected, the monovalent rMeV-BA.1-preS-6P vaccine induced high NAb titers against homologous BA.1 pseudotyped virus, 73.1-fold greater than against D614G ($P < 0.01$), which includes an antibody escape mutation conserved in most SARS-CoV-2 VoCs. However, these antibodies neutralized the Delta pseudotyped virus poorly (0.95-fold, $P > 0.05$) and BA.4/5 pseudotyped virus only modestly (2.9-fold, $P > 0.05$) compared to D614G (Fig. 3*H*).

Interestingly, the trivalent vaccine induced a slightly greater, 1.5-fold, NAb activity against BA.1 compared to the monovalent vaccine (Fig. 3*H*). But the NAb response to the trivalent vaccine was much broader with 88.5-fold, 25-fold, and 13.1-fold higher NT_{50} against the D614G, Delta, and BA.4/5 pseudotyped viruses, respectively (Fig. 3*H*). Compared to D614G, these sera had a significantly reduced NAbs against Delta ($P < 0.05$) but not BA.1 or BA.4/5 ($P > 0.05$). Overall, the trivalent vaccine induced higher and much broader NAbs than the monovalent vaccine.

Serum IgG Antibody Responses to Trivalent and Monovalent Vaccines Are Retained for at least Four Months. Mice immunized with the lower dose (5×10^5 PFU) were used to determine the longevity of antibody response (Fig. 4*A*). For both monovalent and trivalent vaccines, high levels of WA1 and BA.1 S-specific IgG responses (Fig. 4 *B* and *C*) were detected as early as week 2 and reached a peak titer at weeks 5 or 7 and maintained that level for at least 16 wk. WA1 S-specific IgG titers induced by the trivalent vaccine were significantly higher than those in monovalent vaccine (Fig. 4*B*). No significant difference in BA.1 S-specific IgG titers was observed between trivalent and monovalent vaccine groups

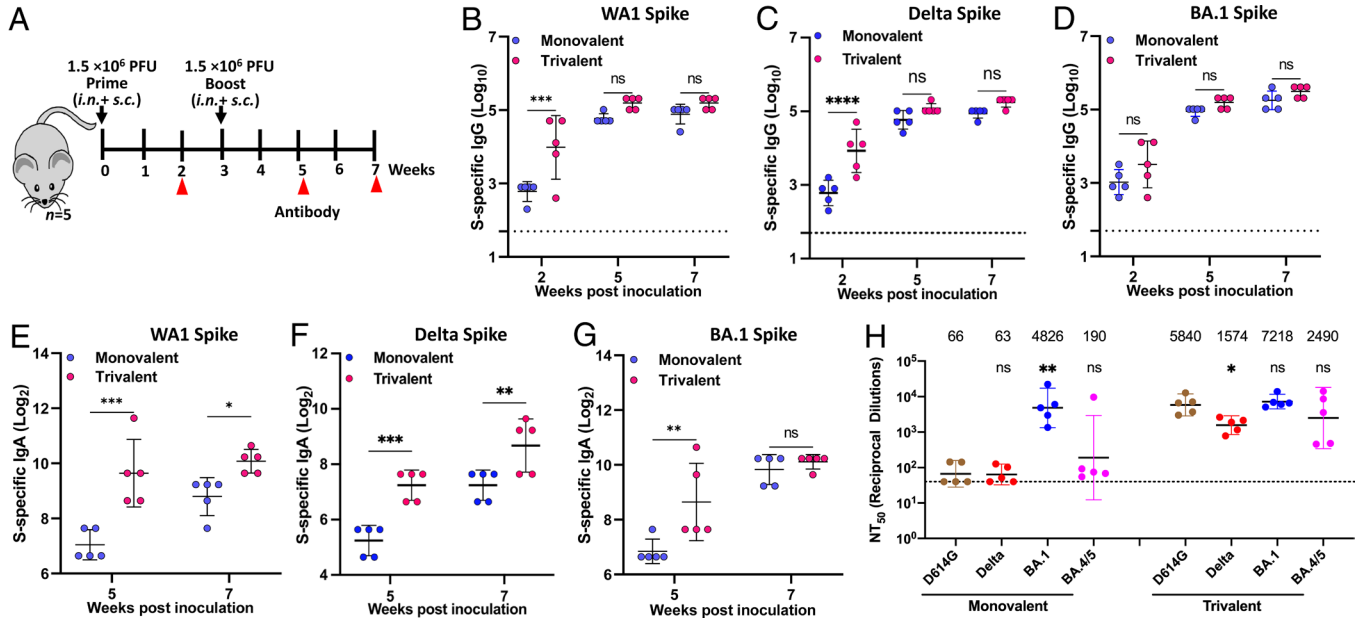

Fig. 3. Immunogenicity of monovalent and trivalent vaccines in IFNAR1$^{-/-}$ mice at doses of 1.5 × 10^6 PFU. (*A*) Immunization schedule. IFNAR1$^{-/-}$ mice (n = 5) were immunized with a high dose (1.5 × 10^6 PFU) of monovalent or trivalent vaccine via a combination of *i.n.* and *s.c.* routes and were boosted three weeks later. Sera were collected for determination of SARS-CoV-2 WA1 (*B*), Delta (*C*), or BA.1 (*D*) S-specific IgG titer measured by ELISA, and SARS-CoV-2 WA1 (*E*), Delta (*F*), or BA.1 (*G*) S-specific IgA titer measured by ELISA. (*H*) NAbs against different SARS-CoV-2 VoCs. Sera at week 7 were used for pseudotype neutralization assay against SARS-CoV-2 D614G, Delta, Omicron BA.1, or BA.4/5 spike. Data are expressed as the mean of five mice ± SD. Dotted line indicates the limit of detection (LOD). Data were analyzed using Student's *t*-test (*P < 0.05; **P < 0.01; ***P < 0.001; ****P < 0.0001).

(Fig. 4*C*). No significant difference was observed for WA1 S-specific IgG between low and high doses for both trivalent and monovalent vaccines (Fig. 4*D*). BA.1 S-specific IgG was significantly higher in the high dose than in the low dose for the trivalent vaccine, whereas no difference was observed between low and high doses for the monovalent vaccine (Fig. 4*E*). Therefore, a low-dose immunization is sufficient to induce a strong serum IgG, which can last for at least 4 mo.

Trivalent and Monovalent Vaccine Immunization Induces Respiratory Tissue-Resident Memory T Cell Responses. Recent evidence indicates a critical role for mucosal tissue-resident memory T cells (T_{RM}) in protection against SARS-CoV-2 infection (24, 25). To separate the tissue-resident and circulating T cells in the lungs, anti-CD45-PE was injected into mice 10 min before they were killed. Lung T cell suspensions were isolated and stimulated with phorbol myristate acetate (PMA)/ionomycin or a S-specific peptide pool. The cells were stained with antibodies specific for T cell lineages (i.e., CD4 or CD8) and activation status (i.e., CD62L, CD44, or CD69). Subsequently, cells were fixed and permeabilized, stained with anti-cytokine antibodies (anti-IFN-γ, anti-IL-17, and anti-IL-5 for CD4$^+$ T cells or anti-IFN-γ for CD8$^+$ T cells), and analyzed by flow cytometry. Gating strategy for flow cytometry analysis is depicted in *SI Appendix*, Fig. S2 and S3.

Within the CD45$^-$ tissue-resident memory T cell (T_{RM}) population, the percentage (Fig. 5*A*) and number (Fig. 5*B*) of S-specific CD4$^+$CD44$^+$CD62L$^-$CD69$^+$ antigen–positive T cells increased significantly in mice immunized with monovalent or trivalent vaccine compared to the MMM control. However, there was no significant difference between monovalent and trivalent vaccine groups (P > 0.05). IFN-γ-producing cells (Fig. 5 *C* and *D*) in trivalent vaccine–immunized mice were higher in both vaccine candidates but were not significantly different from the MMM control. The percentage and number of IL-17-producing cells (Fig. 5 *E* and *F*) significantly increased in mice immunized with monovalent or trivalent vaccine (P < 0.01 or P < 0.001). In addition, IL-5-producing cells (Fig. 5 *G* and *H*) were detected in 2 out of 5 mice in trivalent vaccine–immunized mice but were not detected in monovalent vaccine or MMM control. When CD45$^-$ CD4$^+$ T cells were stimulated with PMA/ionomycin, a similar but slightly different pattern was observed (*SI Appendix*, Fig. S4). Specifically, the percentage and number of total CD4$^+$CD44$^+$CD62L$^-$CD69$^+$ cells (*SI Appendix*, Fig. S4 *A* and *B*) in both monovalent and trivalent vaccine groups were significantly higher than the MMM control. Additionally, the percentage and/or number of IFN-γ (*SI Appendix*, Fig. S4 *C* and *D*), IL-17 (*SI Appendix*, Fig. S4 *E* and *F*), and IL-5 (*SI Appendix*, Fig. S5 *G* and *H*) producing cells in mice immunized with both vaccines were significantly higher than those in MMM control.

For the CD45$^+$ (circulating) T cell populations, there was an overall increase in the percentage and number of S-specific CD4$^+$CD44$^+$CD62L$^-$CD69$^+$ cells (*SI Appendix*, Fig. S5 *A* and *B*) but was not significantly different from the MMM control. The percentage and number of S-specific IFN-γ (*SI Appendix*, Fig. S5 *C* and *D*), IL-17 (*SI Appendix*, Fig. S5 *E* and *F*), and IL-5-producing CD45$^+$ cells (*SI Appendix*, Fig. S5 *G* and *H*) were higher in the trivalent than the monovalent vaccine group and MMM control, but no significant difference was observed between these groups. When the lung cells were stimulated with PMA/ionomycin, the percentage of CD4$^+$CD44$^+$CD62L$^-$CD69$^+$ cells (*SI Appendix*, Fig. S5 *I* and *J*) was significantly higher in both monovalent and trivalent vaccines compared to the MMM control. In addition, the percentage and number of IL-17-producing CD45$^+$ cells (*SI Appendix*, Fig. S5 *M* and *N*) were significantly higher in trivalent vaccine and monovalent vaccine groups than the MMM control. However, the percentage and number of IFN-γ (*SI Appendix*, Fig. S5 *K* and *L*) and IL-5-producing CD45$^+$ cells (*SI Appendix*, Fig. S5 *O* and *P*) were higher in both trivalent and monovalent vaccine groups but were not significantly different from the MMM control.

We also analyzed tissue-resident and circulating CD8$^+$ T cells. For tissue-resident CD45$^-$CD8$^+$ T cells, the percentage and/or number of S-specific CD8$^+$CD44$^+$CD62L$^-$CD69$^+$ T cells (Fig. 5 *I* and *J*) and IFN-γ producing T cells (Fig. 5 *K* and *L*) were significantly

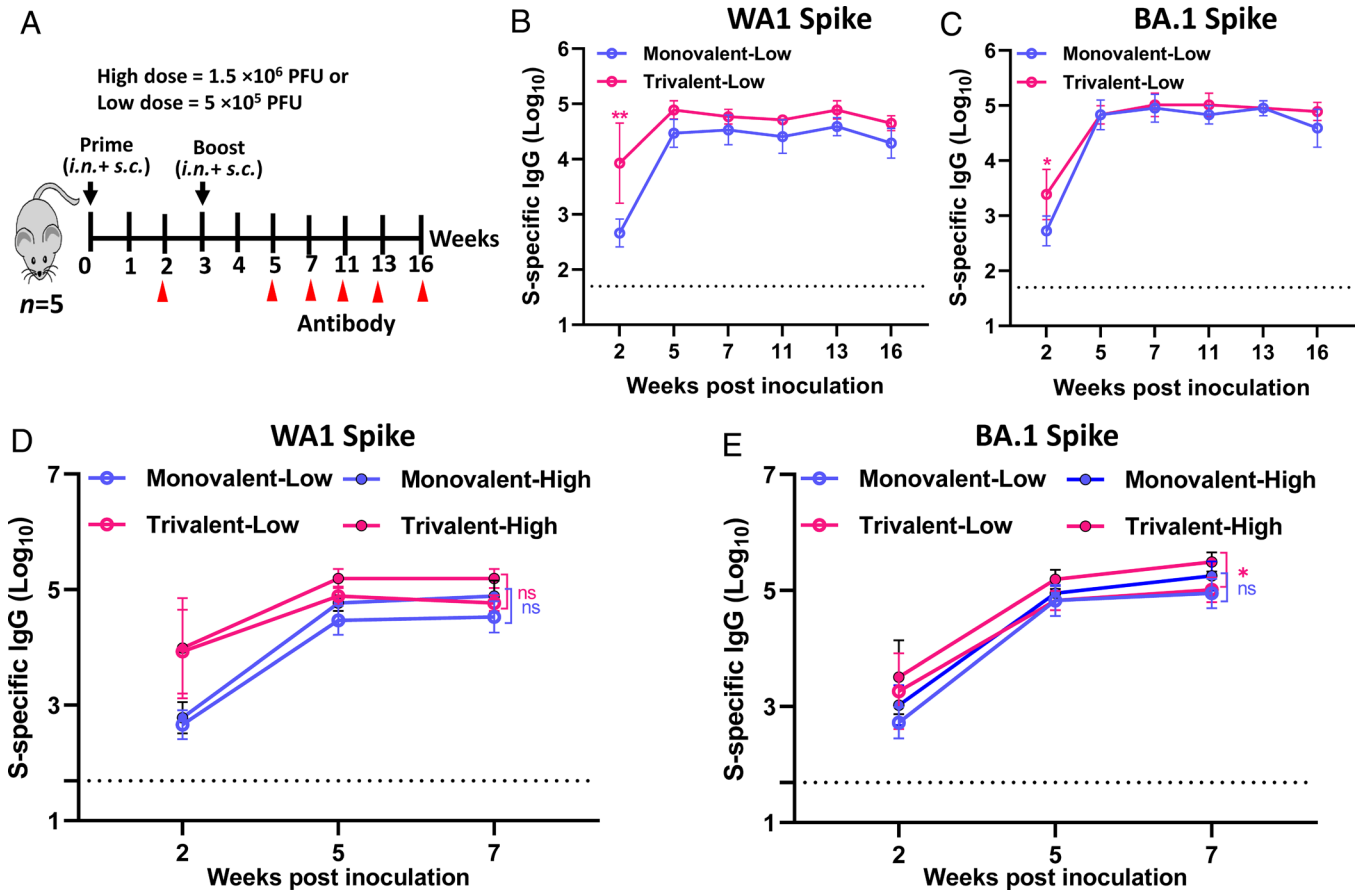

Fig. 4. Durability of antibody responses of monovalent and trivalent vaccines in IFNAR1$^{-/-}$ mice. (*A*) Immunization schedule. IFNAR1$^{-/-}$ mice (n = 5) were immunized with a low (5 × 10^5 PFU) or high (1.5 × 10^6 PFU) dose of monovalent or trivalent vaccine via a combination of *i.n.* and *s.c.* routes and were boosted three weeks later. (*B*) Dynamic of WA1 S-specific IgG titers. (*C*) Dynamic of BA.1 S-specific IgG titers. (*D* and *E*) Comparison of WA1 (*D*) and BA.1 (*E*) S-specific IgG between low and high dose immunization. Data are expressed as the mean of five mice ± SD. Dotted line indicates the limit of detection (LOD). Data were analyzed using two-way ANOVA (*P < 0.05).

higher in mice immunized with monovalent or trivalent vaccine compared to the MMM control. However, there was no significant difference between monovalent and trivalent vaccine groups (P > 0.05). A similar pattern (*SI Appendix*, Fig. S6 *A–D*) was observed in the $CD45^-CD8^+$ T cells following stimulation with PMA/ionomycin. Stimulation of lung cells with the S peptide pool detected an overall increase in $CD45^+CD8^+CD44^+CD62L^-$ $CD69^+$ T cells (*SI Appendix*, Fig. S7 *A* and *B*) in both monovalent and trivalent vaccines, but the increase did not differ from the MMM control. Importantly, S-specific IFN-γ producing $CD8^+$ T cells (*SI Appendix*, Fig. S7 *C* and *D*) were significantly higher in the trivalent vaccine–immunized mice than in mice immunized with the monovalent vaccine and MMM control. When stimulating with PMA/ionomycin, the percent and/or number of $CD8^+CD44^+CD62L^-CD69^+$ T cells (*SI Appendix*, Fig. S7 *E* and *F*) and IFN-γ-producing T cells (*SI Appendix*, Fig. S7 *G* and *H*) were significantly higher in mice immunized with monovalent or trivalent vaccine compared to the MMM control. Therefore, both monovalent and trivalent vaccines are capable of inducing antigen-specific $CD8^+$ cells, and the trivalent vaccine induces higher antigen-specific IFN-γ-producing $CD8^+$ T cells than the monovalent vaccine.

The Trivalent Vaccine Induces Stronger Systemic T Cell Responses than the Monovalent Vaccine. At week 7 postimmunization, splenocytes were isolated from mice that were immunized with the high dose (1.5 × 10^6 PFU) of vaccine and stimulated with S peptides for T cell assay. Gating strategy for flow cytometry analysis is depicted in *SI Appendix*, Fig.S8. Th1 cells produce cytokines (i.e., IFN-γ and TNF-α) that help cytotoxic T cells and B cells which are critical for protection against SARS-CoV-2 infection. Flow cytometry analysis of $CD3^+CD4^+$ cells producing Th1 cytokines showed that splenocytes isolated from monovalent and trivalent vaccine groups but not from the MMM group expressed SARS-CoV-2 S-specific IFN-γ (Fig. 6 *A* and *B*) producing T helper cells ($CD4^+$IFN-γ^+). Interestingly, more TNF-α-producing T helper cells ($CD4^+$TNF-α^+) were detected in the splenocytes of mice immunized with trivalent vaccine and monovalent vaccine compared to the MMM control (Fig. 6 *C* and *D*).

Th2 cells produce signature cytokines such as IL-4 and IL-10, which support the antibody production. Interestingly, the trivalent vaccine but not the monovalent vaccine induced significantly more antigen-specific IL-4-producing T helper cells compared to the MMM control (Fig. 6 *E* and *F*). In addition, neither the trivalent vaccine nor the monovalent vaccine induced a significant number of antigen-specific IL-10-producing T helper cells (P > 0.05) (Fig. 6 *G* and *H*).

Interleukin 21, the signature product of follicular T helper cells (T_{FH}), and IL-17, the product of T_H17 cells, facilitate antibody production and affinity maturation. Both trivalent vaccine and monovalent vaccine induced significantly more antigen-specific T_H17 cells compared to the MMM control (Fig. 6 *I* and *J*). Furthermore, the trivalent vaccine group had more IL-17-producing cells than the monovalent vaccine group (P < 0.05) (Fig. 6 *I* and *J*). Both the trivalent and the monovalent vaccines induced significantly

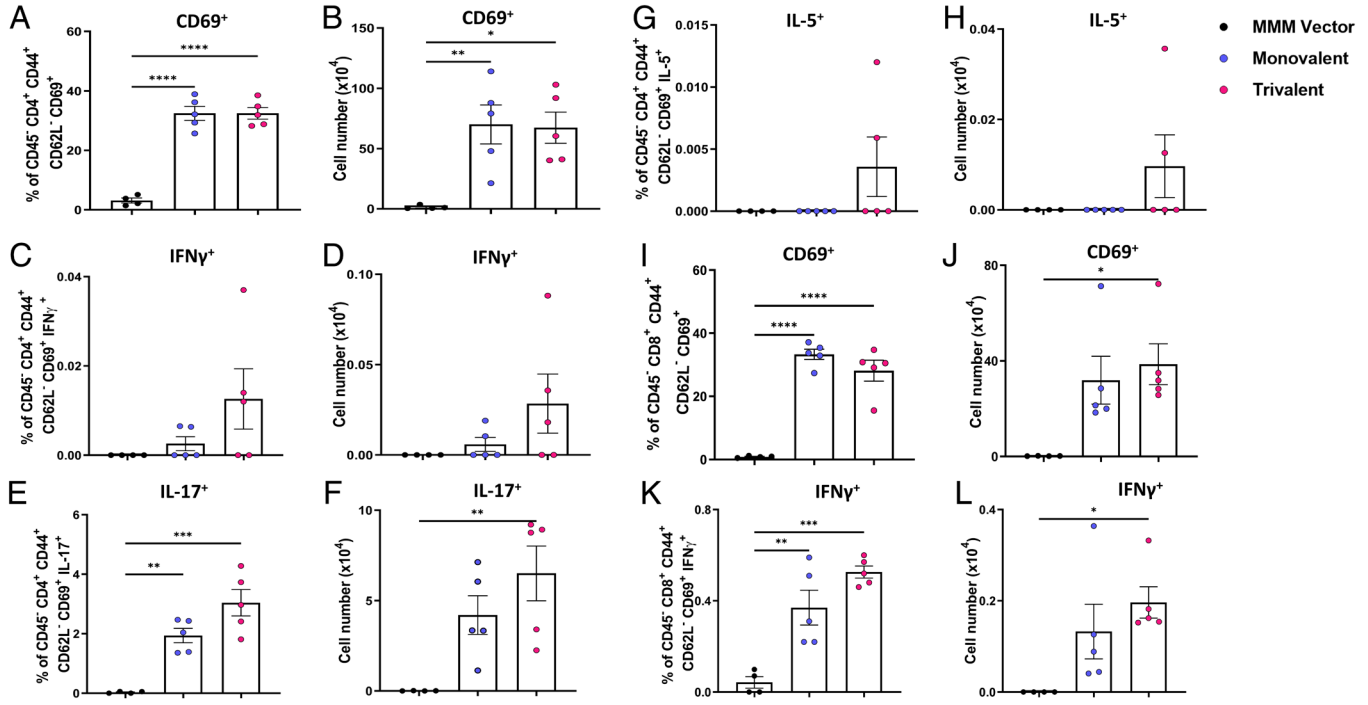

Fig. 5. Monovalent and trivalent vaccines induce S-specific tissue-resident CD4$^+$ and CD8$^+$ T cell immune responses in the lungs. At week 7, immunized IFNAR1$^{-/-}$ mice (n = 5) from Fig. 3 were injected with CD45-PE antibody 10 min before the mice were killed in order to separate the resident (CD45$^-$) and circulating (CD45$^+$) T cells. Lung CD45$^-$ T cell suspensions were stimulated with a WA1 S-specific peptide pool. Cells were surface stained with antibodies specific for CD4 or CD8, CD62L, CD44, and CD69, then fixed, permeabilized, and stained with anti-IFNγ, anti-IL-17, and anti-IL-5 for CD4$^+$ T cells. The percent and number of S-specific CD45$^-$ CD4$^+$CD44$^+$CD62L$^-$CD69$^+$ T cells (*A* and *B*), IFNγ$^+$ (*C* and *D*), IL-17$^+$ (*E* and *F*), and IL-5$^+$ (*G* and *H*) producing CD4$^+$ T cells are shown in *A*–*H*. The CD8$^+$CD69$^+$ T cells in the lungs were stimulated a WA1 S-specific peptide pool (*I*–*L*). The percent and number of S-specific CD45$^-$CD8$^+$CD44$^+$CD62L$^-$CD69$^+$ T cells (*I* and *J*) and IFNγ$^+$-producing CD8$^+$ T cells (*K* and *L*) are shown. One-way ANOVA with Tukey's multiple comparisons was used to detect differences among groups (*P < 0.05; **P < 0.01; ***P < 0.001; ****P < 0.0001).

more antigen-specific IL-21-producing T helper cells compared to the MMM control (Fig. 6 *K* and *L*). All together, trivalent vaccine candidate stimulated a significantly higher systemic T cell immune response compared to the monovalent vaccine.

Trivalent Vaccine Increases and Broadens Neutralization Activity Against SARS-CoV-2 VoCs in Golden Syrian Hamsters. We next assessed the immunogenicity of the trivalent and monovalent vaccines in hamsters (Fig. 7*A*). For both monovalent and trivalent

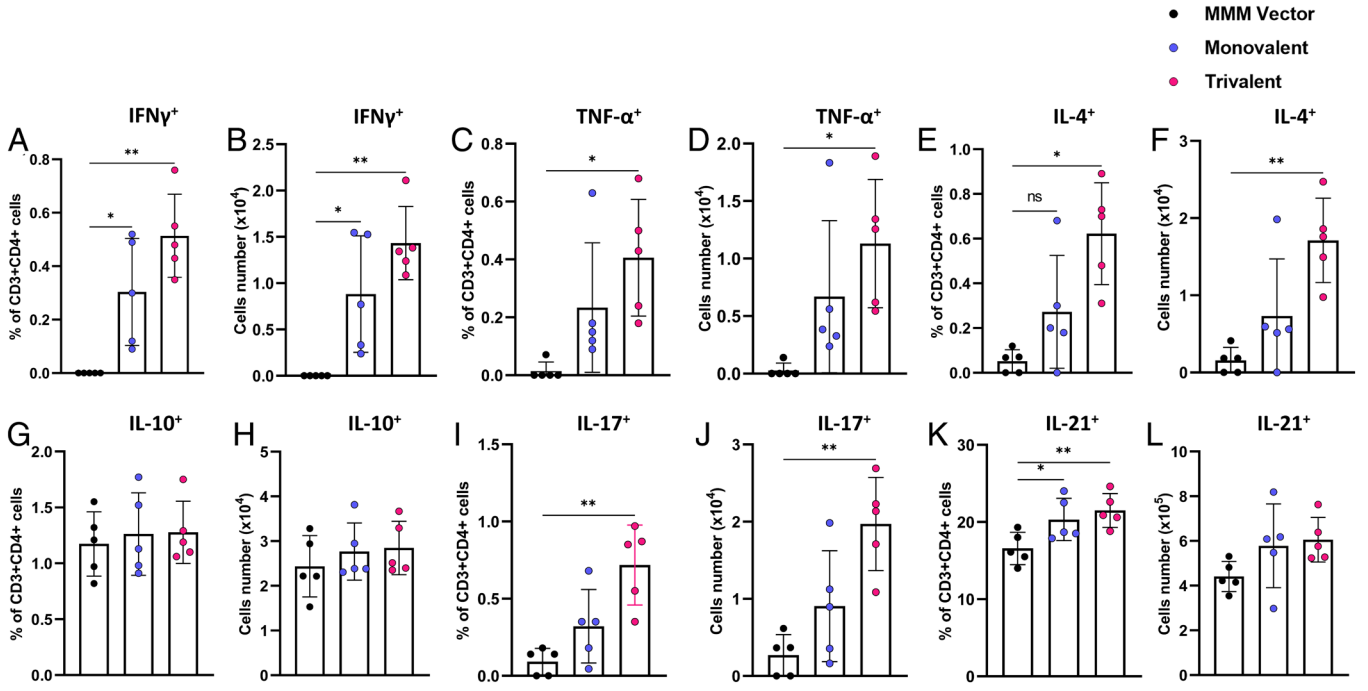

Fig. 6. Monovalent and trivalent vaccines induce systemic T cell response. At week 7, IFNAR1$^{-/-}$ mice (n = 5) from Fig. 3 were killed, and splenocyte suspension was stimulated with 20 μg/mL of WA1 preS protein for 5 d. The frequencies and number of S-specific IFN-γ$^+$CD4$^+$ (*A* and *B*), TNF-α$^+$CD4$^+$ (*C* and *D*), IL-4$^+$CD4$^+$ (*E* and *F*), IL-10$^+$CD4$^+$ (*G* and *H*), IL-17$^+$ CD4$^+$ (*I* and *J*), and IL-21$^+$ CD4$^+$ (*K* and *L*) cells were determined by flow cytometry after intracellular staining with the corresponding anti-cytokine antibody. Data are expressed as mean of five mice ± SD. Data were analyzed using one-way ANOVA (*P < 0.05; **P < 0.01).

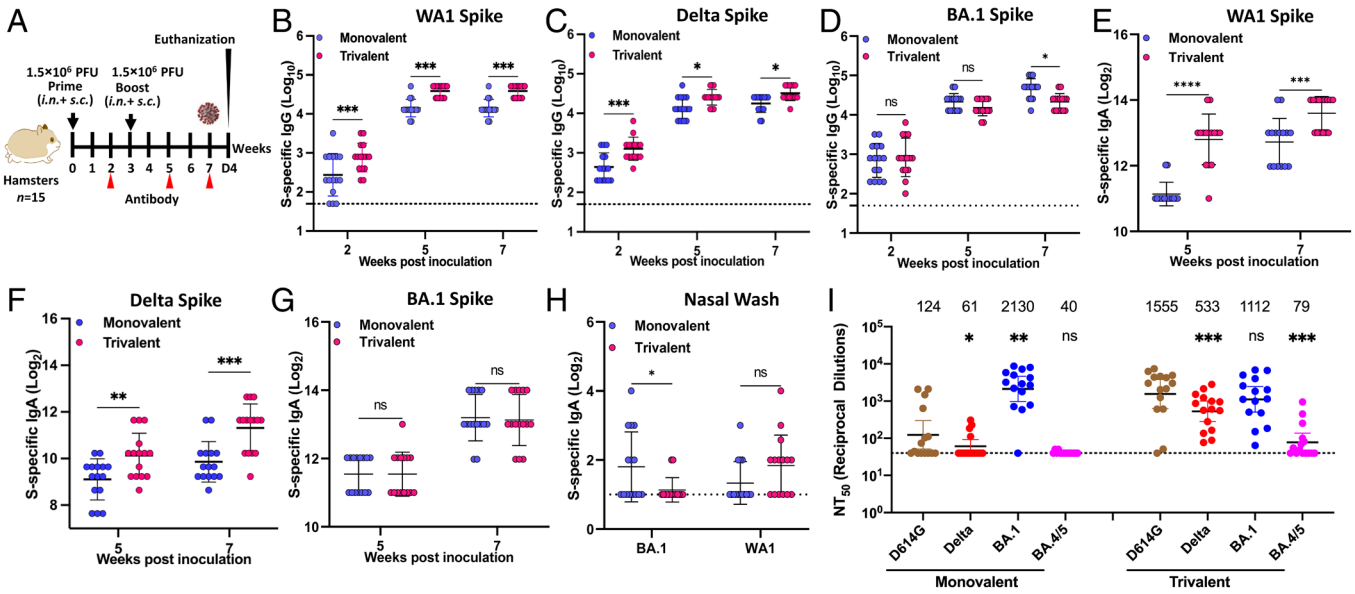

Fig. 7. Characterization of immune responses following monovalent and trivalent immunization in golden Syrian hamsters. (*A*) Immunization schedule in hamsters. Sera were collected for detection of SARS-CoV-2 WA1 (*B*), Delta (*C*), or BA.1 (*D*) S-specific serum IgG titer by ELISA, and SARS-CoV-2 WA1 (*E*), Delta (*F*), or BA.1 (*G*) S-specific serum IgA titer by ELISA. (*H*) BA.1 and WA1 S-specific IgA titer in nasal wash (week 7) measured by ELISA. (*I*) NAbs against different SARS-CoV-2 VoCs. Sera at week 7 were used for the pseudotype neutralization assay against SARS-CoV-2 D614G, Delta, Omicron BA.1, or BA.4/5 spike. Data are the mean of fifteen hamsters ± SD. Dotted line indicates the limit of detection (LOD). Data were analyzed using Student's *t*-test (ns > 0.05, **P* < 0.05; ***P* < 0.01; ****P* < 0.001; *****P* < 0.0001).

vaccines, a high level of serum IgG was detected at week 2 with further increases at weeks 5 and 7 (Fig. 7 *B*–*D*). The WA1 (Fig. 7*B*) and Delta (Fig. 7*C*) S-specific IgG titer in trivalent vaccine was significantly higher than the monovalent vaccine. Omicron BA.1-specific IgG titers in monovalent vaccine were higher than those in trivalent vaccine, but a statistical difference was only observed at week 7 (Fig. 7*D*). Similarly, a high level of IgA was detected in all serum samples from both the monovalent and the trivalent vaccine groups (Fig. 7 *E*–*G*). WA1 (Fig. 7*E*) and Delta (Fig. 7*F*) S-specific IgA antibodies in the trivalent vaccine group was significantly higher than those in the monovalent vaccine group at weeks 5 and 7. However, there was no significant difference in BA.1 S-specific IgA titer between trivalent and monovalent vaccines (Fig. 7*G*).

S-specific IgA in nasal wash was also detected in some but not all hamsters in both vaccine groups (Fig. 7*H*). Only 7/15 hamsters in the monovalent vaccine group produced BA.1 S-specific IgA, and only 4 produced WA1 S-specific IgA. Only 2/15 hamsters in the trivalent vaccine group produced BA.1 S-specific IgA, whereas 9/15 produced WA1 S-specific IgA.

Sera at week 7 were used to quantify NAbs against D614G, Delta, Omicron BA.1, or BA.4/5 using the pseudotype neutralization assay (Fig. 7*I*). Similar to the mouse sera, the monovalent vaccine induced high NAb titers against BA.1, but much lower neutralizing activity for D614G and Delta variant, and below the limit of detection for BA.4/5. The trivalent vaccine sera neutralized BA.1 slightly (0.5-fold) less efficiently than the monovalent rMeV-BA.1-preS-6P vaccine, while it had 12.5-, 8.7-, 1.9-fold increase in neutralizing activity against D614G, Delta, and BA.4/5, respectively, compared to the monovalent vaccine. Thus, the trivalent vaccine induces robust, broader NAbs against D614G, Delta, and Omicron BA.1 strains, whereas the monovalent vaccine sera only efficiently neutralize the homologous Omicron BA.1, but not the D614G, Delta, or BA.4/5 heterologous strains.

Trivalent MMS Vaccine Enhances and Broadens Protection against SARS-CoV-2 Infection. At week 7, the 15 hamsters in each group were each divided into 3 subgroups (n = 5) and challenged with SARS-CoV-2 WA1, the Delta, or the Omicron BA.1, respectively.

After challenging with 2×10^4 PFU of SARS-CoV-2 WA1, the monovalent vaccine and trivalent vaccine groups did not have significant weight loss ($P > 0.05$) (Fig. 8*A*). At day 4 postchallenge, 6.7 and 7 $\log_{10}$ PFU/g tissue of SARS-CoV-2 were detected in the lungs and nasal turbinates of the MMM vector group, respectively (Fig. 8 *B* and *C*). The SARS-CoV-2 titer was significantly reduced by immunization with the monovalent vaccine group to approximately 3.0 and 4.4 $\log_{10}$ PFU/g tissue in lungs and nasal turbinate, respectively (Fig. 8 *B* and *C*). Notably, the SARS-CoV-2 titer in the lungs and nasal turbinate of the trivalent vaccine group was below or near the detection limit (Fig. 8 *B* and *C*). All five lungs in the MMM vector group had severe histological changes (an average score of 3.1) characterized by extensive pneumonia (Fig. 8*D* and *SI Appendix*, Fig. S9). In contrast, only mild lung histological changes were detected in the trivalent vaccine group (an average score of 0.8), which was significantly less than the monovalent vaccine group (average score of 1.6) ($P < 0.05$) (Fig. 8*D* and *SI Appendix*, Fig. S9). Therefore, the trivalent vaccine provided better protection against a SARS-CoV-2 WA1 challenge than the monovalent vaccine.

After challenging with 2×10^4 PFU of the SARS-CoV-2 Delta, hamsters in the MMM vector group had approximately 7% weight loss by day 4 ($P < 0.01$) (Fig. 8*E*). The monovalent vaccine group showed less weight loss (3%, $P < 0.05$), and no weight loss was observed in the trivalent vaccine group ($P > 0.05$) (Fig. 8*E*). The MMM vector immunized hamsters had high viral burden in lungs and nasal turbinates (approximately 6 log10 PFU/g tissue), while the lungs and nasal turbinates in the monovalent vaccine group were 2.7 and 3.4 log10 PFU/g tissue, and the level of virus in the lung and nasal turbinate of the trivalent vaccine group was below the detection limit (Fig. 8 *F* and *G*). Lungs from the MMM vector group had severe pneumonia with an average score of 3.5 (Fig. 8*H* and *SI Appendix*, Fig. S10). The lung pathology in the monovalent vaccine group was reduced but significant (average score of 2.2), while lung tissues from the trivalent vaccine group only had mild

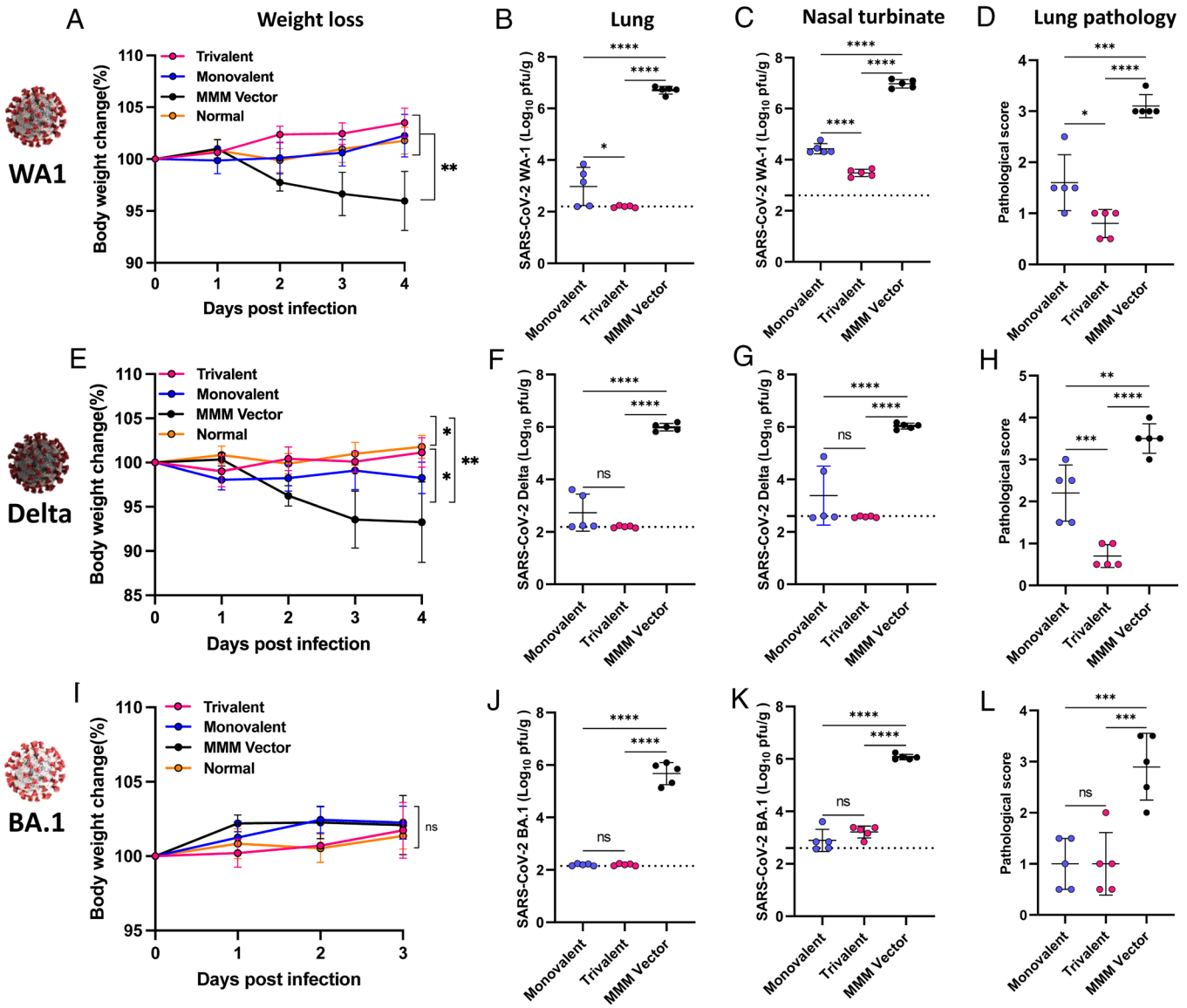

Fig. 8. The trivalent vaccine provides broader protection against SARS-CoV-2 challenge in golden Syrian hamsters than the monovalent vaccine. Hamsters (n = 5) from Fig. 7. were challenged with 2×10^4 PFU SARS-CoV-2 WA1 (*A–D*), or Delta variant (*E–H*), or 7×10^5 PFU of Omicron BA.1 (*I–L*). (*A*) Body weight changes in hamsters. (*B* and *C*) SARS-CoV-2 titer in the lung (*B*) and nasal turbinate (*C*) at day 4. (*D*) Lung pathology score after challenge with SARS-CoV-2 WA1. Each lung section was scored based on the severity of histologic changes. Score 4, extremely severe; score 3, severe; score 2, moderate; score 1, mild; score 0, no pathological changes. (*E*) Body weight changes in hamsters. (*F* and *G*) SARS-CoV-2 titer in the lung (*F*) and nasal turbinate (*G*) at day 4. (*H*) Lung pathology score. (*I*) Body weight changes in hamsters. (*J* and *K*) SARS-CoV-2 titers in the lung (*J*) and nasal turbinate (*K*) at day 3. (*L*) Lung pathology score. Dotted line indicates the limit of detection (LOD). Data were analyzed using two-way ANOVA and one-way ANOVA (ns, not significant; *$P < 0.05$; **$P < 0.01$; ***$P < 0.001$; ****$P < 0.0001$).

pathological changes with an average score of 0.7 (Fig. 8*H* and *SI Appendix*, Fig. S10). Thus, the trivalent vaccine provided complete protection against challenge with SARS-CoV-2 Delta, whereas monovalent vaccine provided substantial but not complete protection.

For Omicron BA.1 challenge, hamsters were first transduced by *i.n.* administration of 10^8 PFU of adenovirus serotype 5 expressing human ACE2 receptor (Ad5-hACE2) 5 d prior to challenge with 7×10^5 PFU of the Omicron BA.1 variant. None of the hamster groups displayed significant weight loss ($P > 0.05$) (Fig. 8*I*). As expected, the monovalent vaccine group showed sufficient protection against its homologous virus challenge (Fig. 8 *J* and *K*). Of note, the trivalent vaccine showed a comparable level of protection against BA.1 challenge as the monovalent vaccine (Fig. 8 *J* and *K*). The SARS-CoV-2 titer in both groups was below or near the detection limit. Lung histology showed that the MMM vector group had moderate to severe pneumonia with an average score of 2.9 (Figs. 8*L* and 9). However, lung pathology in both monovalent and trivalent vaccine groups was mild (score of 1.0) ($P > 0.05$) (Figs. 8*L* and 9). Thus, both monovalent and trivalent vaccines provide complete protection against Omicron BA.1 infection in hamsters.

Intranasal Immunization of Trivalent MMS Vaccine Provides Complete Protection against SARS-CoV-2 Infection. To determine whether intranasal immunization alone can provide protection against SARS-CoV-2 infection, hamsters (n = 15) were immunized *i.n.* with 1.5×10^6 PFU of the trivalent vaccine or MMM vector and were boosted *i.n.* 2 wk later. All 15 hamsters in the trivalent vaccine group induced uniformly high serum S-specific IgG (Fig. 10 *A–C*) and IgA (Fig. 10 *D–F*) antibody titers against SARS-CoV-2 WA1, Delta, and Omicron BA.1 variant. At week 7, 5 hamsters in each group were challenged with SARS-CoV-2 WA1 (Fig. 10 *G–I*), Delta (Fig. 10 *J–L*), and Omicron BA.1 variant (Fig. 10 *M–O*), respectively. Hamsters in the trivalent vaccine group did not have

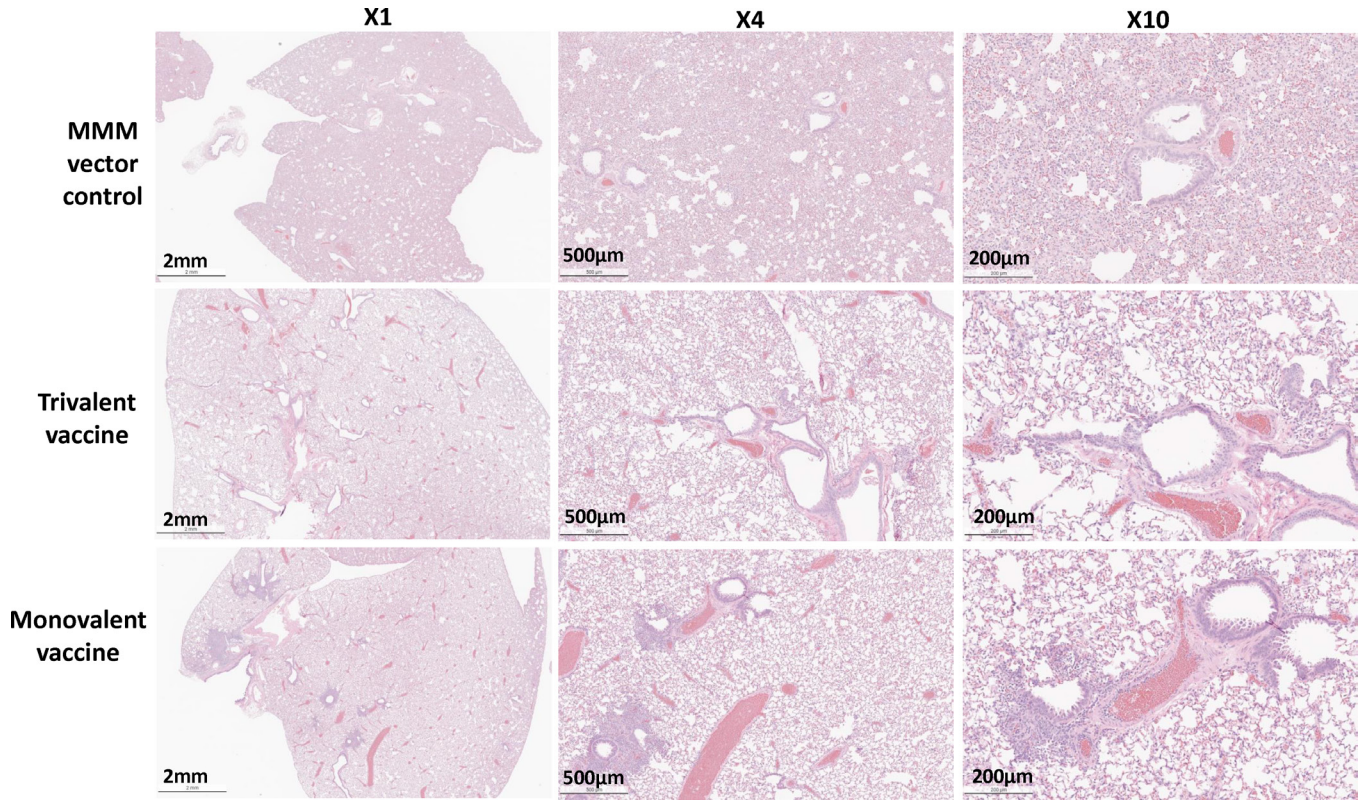

Fig. 9. Monovalent and trivalent vaccine immunization protects against lung pathology after challenge with Omicron BA.1. Hamsters were killed at day 3 after challenge with the SARS-CoV-2 BA.1 variant. Lung tissue was stained with hematoxylin/eosin and examined histologically. Micrographs with 1×, 4×, and 10× magnification of a representative lung section from each group are shown.

any weight loss (Fig. 10 *G*, *J*, and *M*), whereas MMM vector control had 7% and 5% weight loss after challenge with SARS-CoV-2 WA1 and Delta variants, respectively. SARS-CoV-2 titers in lung and nasal turbinate were below the detection limit after challenge with SARS-CoV-2 WA1 (Fig. 10 *H* and *I*), Delta (Fig. 10 *K* and *L*), and Omicron BA.1 variant (Fig. 10 *N* and *O*). Thus, *i.n.* immunization with the trivalent MMS vaccine provides complete protection against all three SARS-CoV-2 viruses.

Intranasal Immunization of Trivalent Vaccine Leads to a Significantly Higher Serum IgG Antibody Response Compared to Subcutaneous Immunization. We next compared the immune responses between *i.n.* and *s.c.* immunization routes. Briefly, IFNAR1$^{-/-}$ mice (n = 10) were immunized with 1.2 × 10^6 PFU of the trivalent vaccine candidate via the *i.n.* or *s.c.* route and were boosted two weeks later (Fig. 11*A*). The magnitude of WA1 S-, Delta S-, and Omicron BA.1 S-specific serum IgG responses in the *i.n.* immunization group was significantly higher than that of the *s.c.* immunization group at all three time points and sustained for at least 6 wk (Fig. 11 *B*–*D*). Likewise, WA1 S-, Delta S-, and Omicron BA.1 S-specific IgG titers in lung bronchoalveolar lavage (BAL) at week 6 in the *i.n.* immunization group were significantly higher than those in the *s.c.* immunization group (Fig. 11*E*). Thus, *i.n.* immunization of trivalent vaccine induces stronger S-specific IgG than *s.c.* immunization in sera and lungs.

Intranasal but Not Subcutaneous Immunization of Trivalent Vaccine Induces a Mucosal IgA Antibody Response. The above sera and BAL were also tested for an S-specific IgA response. Importantly, *i.n.* immunization induced a high level of mucosal WA1 S-, Delta S-, and Omicron BA.1 S-specific IgA in serum (Fig. 11 *F*–*H*) and BAL (Fig. 11*I*) that increased over time. In contrast, IgA titers were below the detection limit in both serum (Fig. 11 *F*–*H*) and BAL samples (Fig. 11*I*) from the *s.c.* immunization group. Therefore, intranasal immunization with the trivalent vaccine induces a superior antibody response both systemically and locally in the lung relative to the subcutaneous route.

MeV and MuV Vectors Do Not Interfere with the S-Specific Antibody Induced by rMuV-JL1-Delta-preS-6P. IFNAR1$^{-/-}$ mice were immunized *i.n.* with a high dose (1.5 × 10^6 PFU) of trivalent vaccine, rMuV-JL1-Delta-preS-6P, a mixture of rMuV-JL1-Delta-preS-6P, rMuV-JL2 vector, and rMeV vector, or a low dose (5 × 10^5 PFU) of rMuV-JL1-Delta-preS-6P. Mice were boosted with the same vaccine at the same dose three weeks later. First, all immunization groups induced high IgG titers against SARS-CoV-2 WA1, Delta variant, and Omicron BA.1 (*SI Appendix*, Fig. S11 *A*–*C*). Second, at the same dose (1.5 × 10^6 PFU), trivalent vaccine induced higher IgG titer than rMuV-JL1-Delta-preS-6P alone and a mixture of rMuV-JL1-Delta-preS-6P, rMuV-JL2, and rMeV vector (*SI Appendix*, Fig. S11 *A*–*C*). However, they were not statistically different between each other (P > 0.05). Third, within the two rMuV-JL1-Delta-preS-6P groups, high (1.5 × 10^6 PFU) and low (5 × 10^5 PFU) doses induced similar IgG titers against preS-6P of Delta variant and Omicron BA.1. However, a high dose of rMuV-JL1-Delta-preS-6P induced stronger IgG titer than a low dose immunization against preS-6P of SARS-CoV-2 WA1. These results suggest that rMuV and rMeV vectors do not significantly interfere with their ability to induce S-specific antibody.

Discussion

Here, we developed an intranasal trivalent MMS vaccine candidate that can protect against three major diseases—measles, mumps,

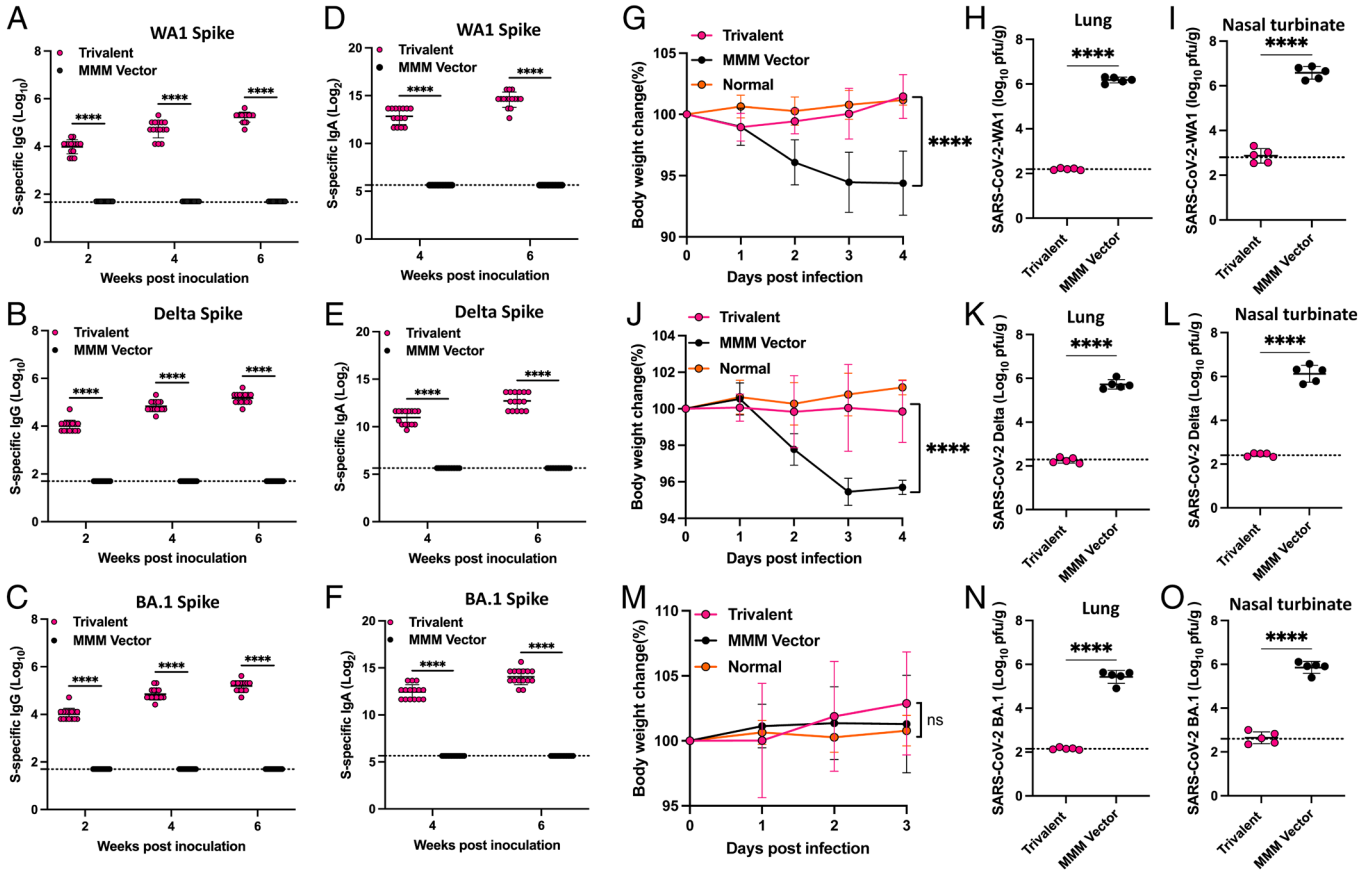

Fig. 10. Intranasal immunization of trivalent vaccine provides complete protection against SARS-CoV-2 challenge in golden Syrian hamsters. Hamsters immunized *i.n.* with 1.5×10^6 PFU of trivalent vaccine or parental MMM vector and were boosted *i.n.* 2 wk later. SARS-CoV-2 WA1 (*A*), Delta (*B*), or BA.1 (*C*) S-specific IgG was determined by ELISA. SARS-CoV-2 WA1 (*D*), Delta (*E*), or BA.1 (*F*) S-specific IgA was determined by ELISA. At week 7, hamsters were challenged with 2×10^4 PFU SARS-CoV-2 WA1 (*G–I*), or Delta variant (*J–L*), or 7×10^5 PFU of Omicron BA.1 (*M–O*). (*G*) Body weight changes, SARS-CoV-2 titer in the lung (*H*), and nasal turbinate (*I*) in hamsters after challenge with SARS-CoV-2 WA1. (*J*) Body weight changes, SARS-CoV-2 titer in the lung (*K*), and nasal turbinate (*L*) in hamsters after challenge with the Delta variant. (*M*) Body weight changes, SARS-CoV-2 titer in the lung (*N*), and nasal turbinate (*O*) in hamsters after challenge with Omicron BA.1 variant. Dotted line indicates the limit of detection (LOD). Data were analyzed using two-way ANOVA and one-way ANOVA (ns, not significant; $*P < 0.05$; $**P < 0.01$; $***P < 0.001$; $****P < 0.0001$).

and multiple SARS-CoV-2 VoCs—in a single vaccine. The trivalent vaccine candidate induces high levels of SARS-CoV-2-specific serum IgG antibody, broadened NAbs, robust mucosal IgA, and strong systemic and lung resident T cell responses that provide complete protection against challenge with ancestral SARS-CoV-2 and different VoCs including Delta and Omicron BA.1 variants. Thus, our MMS vaccine candidate is a promising next-generation COVID-19 vaccine.

Our MMS vaccine candidate has several distinct characteristics. The MMS is a modification of the MMR vaccine, which is safe and highly efficacious, and induces long-term protective immunity. Mice immunized with 5×10^5 PFU of the MMS vaccine generated a high level of S-specific IgG antibody which lasted for at least 4 mo. Sera from MMS vaccine-immunized mice and hamsters had broadened NAbs against the ancestral SARS-CoV-2, D614G mutation, Delta, and Omicron BA.1, and BA.4/5 variants. In contrast, the BA.1 preS-6P-based monovalent vaccine candidate only neutralized the homologous BA.1 strain but not the D614G mutation or other VoCs. Hamsters immunized with the MMS vaccine were completely protected against challenge with the original SARS-CoV-2 WA1 strain and Delta and Omicron BA.1 VoCs. In contrast, the monovalent vaccine only provided sufficient protection against the homologous BA.1 strain, not against the heterologous SARS-CoV-2 WA1 strain or Delta variant. Clearly, inclusion of three preS-6P proteins from three different SARS-CoV-2 strains broadens NAbs and protective response. Another unique advantage of our trivalent MMS vaccine platform is that it can be easily modified and adapted to include newly emerging VoCs by simply exchanging one of the preS-6P proteins for those of the new VoCs, e.g., Omicron subvariants XBB.1.5 and XBB.1.16.

To mimic the formulation of MMR vaccine, we chose to use three vectors to deliver three preS-6P proteins. Although the primary target of both MeV and MuV is the respiratory tract, they have different host tropism and may infect different tissues, organs, and cell types. Interestingly, trivalent vaccine not only induces a higher and broader NAbs but also triggers a higher Th2 cytokine (e.g., IL-4), T_{FH} (IL-21), and T_H17 (IL-17) (Fig. 6) compared to the monovalent vaccine. Perhaps, a combination of MeV, MuV-JL1, and MuV-JL2 expressing multiple preS-6P proteins may offer synergistic effects compared to the rMeV expressing BA.1-preS-6P alone. In addition, we showed that these three vectors do not significantly interfere with each other to induce S-specific antibody. Interestingly, trivalent vaccine induced similar levels of IgG titers against WA1, Delta, and BA.1, whereas it induced a lower Delta S-specific IgA titer in the serum. Perhaps, the lower Delta S-specific IgA titer may lead to a lower Delta S-specific NAbs in the serum. This may be due to the differences in replication kinetics of each virus in vivo, leading to different kinetics of immune responses.

The antigen-specific IgA and T_{RM} are the hallmarks of an effective mucosal vaccine. Intranasal delivery of trivalent vaccine induces strong serum NAbs and mucosal IgA in blood, nose, and lung, as well as $CD4^+$ and $CD8^+$ T_{RM} in the lungs (Fig. 5). All current

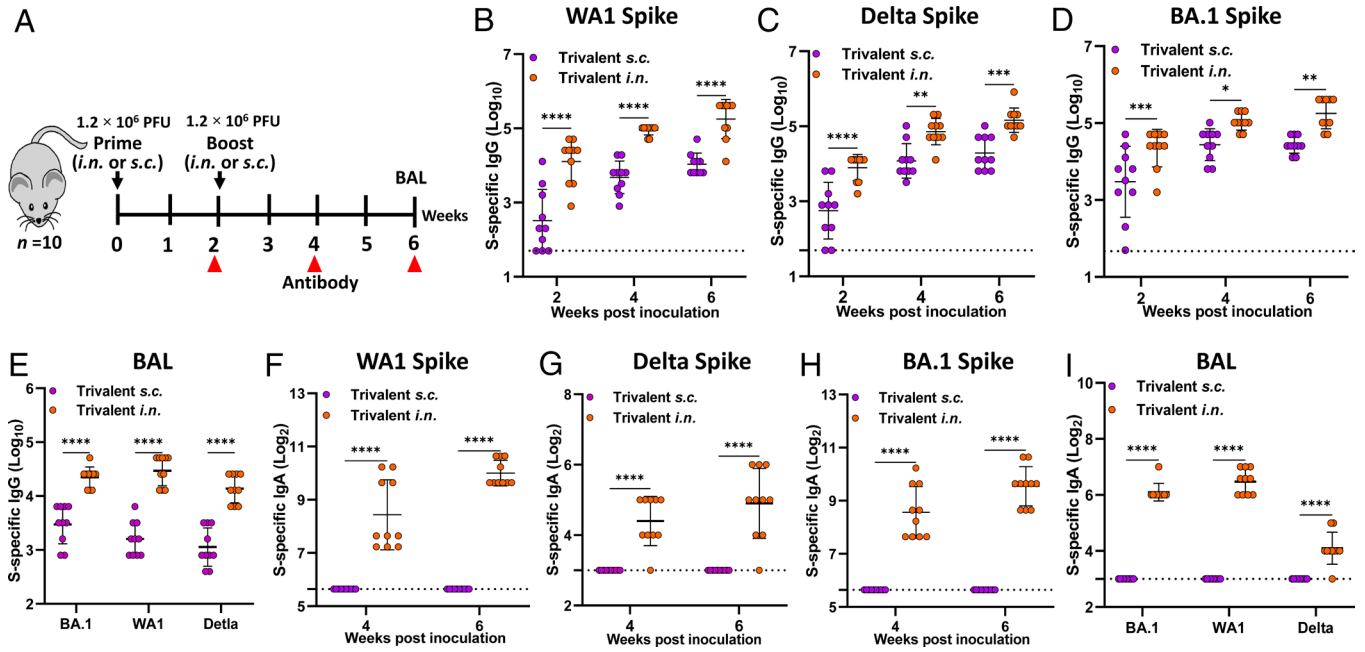

Fig. 11. Comparison of S-specific IgG and IgA responses following intranasal or subcutaneous immunization of trivalent vaccine. (*A*) Experimental schema. (*B*) Serum WA1 S-specific IgG titers. (*C*) Serum Delta S-specific IgG titer. (*D*) Serum BA.1 S-specific IgG titer. (*E*) WA1, Delta, and BA.1 S-specific IgG in the BAL at week 6 postimmunization. (*F*) Serum WA1 S-specific IgA titers. (*G*) Serum Delta S-specific IgA titers. (*H*) Serum BA.1 S-specific IgA titers. (*I*) WA1, Delta, and BA.1 S-specific IgA titer in the BAL at week 6 postimmunization. Dotted line indicates the limit of detection (LOD). Data are expressed as the mean of ten mice ± SD. Statistical differences were determined by Student's *t*-test (*$P < 0.05$, **$P < 0.01$, ***$P < 0.001$, and ****$P < 0.0001$).

COVID-19 vaccines are delivered intramuscularly and induce robust immunity in the blood but lack the mucosal antibody response in the nose and airways (26, 27). Thus, they effectively prevent morbidity and mortality but not prevent infection and transmission as efficiently. The IgA and T_{RM} triggered by MMS vaccine may be capable of preventing both infection and transmission. A vaccine strategy that increases $CD8^+$ T_{RM} cell density in susceptible organs can also provide long-term protection against viruses (28).

Although the standard immunization method for the current MMR vaccine is the subcutaneous or intramuscular route, intranasal delivery of MeV and MuV vaccines has been tested in infants, children, and adults and found to be safe and highly efficacious with additional benefits such as needle-free administration and induction of mucosal immunity (29–32). Therefore, intranasal delivery of MMS vaccine may be feasible for humans. Since both MuV and MeV are neurovirulent (33), evaluation of the neurovirulence of trivalent vaccines in nonhuman primates via intracerebral inoculation may be necessary to ensure the safety of the trivalent vaccine.

The next-generation COVID-19 vaccine should utilize the best SARS-CoV-2 S antigen. Our trivalent vaccine uses preS-6P, the most immunogenic form of the S protein. In contrast, all current COVID-19 vaccines utilize the native full-length S or preS-2P as the vaccine antigen (3). Because preS-6P has much higher protein expression and is more stable compared to preS-2P, the use of preS-6P in vaccine design will significantly enhance the efficacy and longevity of immune responses (18, 20, 22, 34).

In March of 2021, Merck discontinued a MeV-based COVID-19 vaccine (called V591 or TMV-083) because of insufficient immunogenicity (35, 36). In early 2020, they inserted the full-length S with 2 prolines (with deleted furin cleavage site and two mutations in the endoplasmic reticulum retrieval signal) into the H–L gene junction in the MeV Schwarz strain genome. They used V591 in a clinical trial, rather than their best available candidate, rMeV expressing full-length S with 2 prolines and lacking the C-terminal 11 amino acids (MV-ATU2-SF-2P-dER, inserted at P–M gene junction), which were constructed in 2021 (37). Thus, the poor immunogenicity of V591 vaccine is likely due to two factors: the suboptimal design of their full-length preS-2P antigen and the nonoptimal position (H–L rather than P–M gene junction) chosen to insert the S gene into the MeV genome.

One potential concern of using the MMR vaccine platform is the preexisting immunity. Several studies showed that the preexisting MeV immunity had minimal impact on MeV replication and induction of antigen-specific immune responses (38–40). In phase II trial, rMeV-based Chikungunya virus has excellent immunogenicity in the presence of preexisting MeV immunity (41). In the case of Merck's V591 vaccine trial, Launay et al. (36) found that preexisting anti-MeV immunity had a statistically significant impact on the immune response to V591 (36). Perhaps when antigen expression by MeV is low in vivo (e.g., V591), preexisting anti-MeV immunity may interfere with the immune responses against this antigen. For the MuV vector, we previously showed that the preexisting MuV immunity has minimal impact on S-specific antibody induced by rMuV-preS-6P (18).

In summary, we have developed a next-generation COVID-19 vaccine candidate that expresses the most highly optimized S antigen, preS-6P antigen, from the 3 most important SARS-CoV-2 strains delivered intranasally to induce durable mucosal IgA, serum IgG, and lung-resident memory T cell immune responses, thereby providing broad protection against SARS-CoV-2 VoCs.

Materials and Methods

Animal studies were approved by Institutional Laboratory Animal Care and Use Committee at The Ohio State University (protocol no. 2009A1060-R3 and 2020A00000053). Detailed descriptions of virus strains, cell cultures, recovery, and characterization of rMeV, rMuV-JL1, and rMuV-JL2 expressing SARS-CoV-2 preS-6P proteins, multistep growth curves, preparation and purification of large stocks of rMeV and rMuVs, MeV, MuV and SARS-CoV-2 plaque assays, RNA extraction, RT-PCR, Western blot, animal immunization and challenge studies in $IFNAR1^{-/-}$ mice and golden Syrian hamsters, purification of preS-6P protein,

T cell assay, intracellular cytokine staining assay, flow cytometry analysis, ELISA for detection of SARS-CoV-2–specific IgG and IgA antibodies, SARS-CoV-2 neutralizing antibody assay, pseudotype neutralization assay, determination of SARS-CoV-2 titer in mice and hamster tissues, histology, and statistical analysis are provided in *SI Appendix*.

Data, Materials, and Software Availability. All study data are included in the article and/or *SI Appendix*.

ACKNOWLEDGMENTS. This study was supported by startup fund and bridge funding (J.L.) from the Department of Veterinary Biosciences, College of Veterinary Medicine at The Ohio State University and a seed grant (M.E.P. and J.L.) from the Abigail Wexner Research Institute at Nationwide Children's Hospital. This study was in part supported by grants from the NIH (R01AI090060 and R56AI166587 to J.L.; P01 AI112524 to M.E.P. and J.L.; and U19AI42733 to M.E.P.). P.N.B. was supported by NIH grants R01AI145144 and R01AI157205. P.D was supported by R01AI153829. S.-L.L. was supported by NCI U54CA260582. J.X. and Y. Z. were supported by C. Glenn Barber Funds. M.C. was supported by an NIH T32 training grant. M.M.S was supported by a scholarship from the Egyptian Ministry of Education. S.L.L was supported by an anonymous private donor to OSU and by National Cancer Institute U54CA260582. The content is solely the responsibility of the authors and does not necessarily represent the official views of the NIH. We thank Jason McLellan for providing preS-6P genes of SARS-CoV-2 WA1 and Delta variant. We thank Stefan Niewiesk for providing plasmids of the measles virus Edmonston strain for this study. We thank the BSL3 working group and University Laboratory Animal Resources staff at The Ohio State University for their support for this study. We thank members of the J.L. laboratory for technical help and critical readings of the manuscript.

Author affiliations: [a]Department of Veterinary Biosciences, The Ohio State University, Columbus, OH 43210; [b]Department of Microbial Infection and Immunity, College of Medicine, The Ohio State University, Columbus, OH 43210; [c]Department of Microbiology and Immunology, Faculty of Pharmacy, Helwan University, Helwan 11795, Egypt; [d]Center for Vaccines and Immunity, Abigail Wexner Research Institute at Nationwide Children's Hospital, Columbus, OH 43205; [e]Department of Disease Intervention and Prevention, Texas Biomedical Research Institute, San Antonio, TX 78227; [f]Infectious Disease Institute, The Ohio State University, Columbus, OH 43210; [g]Department of Pediatrics, College of Medicine, The Ohio State University, Columbus, OH 43210; and [h]Center for Retrovirus Research, The Ohio State University, Columbus, OH 43210

Author contributions: J.X., Y.Z., P.Q., M.M.S., S.J.Y., J.M., M.L., X.L., P.N.B., M.E.P., S.-L.L., P.D., and J.L. designed research; J.X., Y.Z., P.Q., M.M.S., S.J.Y., J.M., I.T., M.K., J.M.H., J.P.E., M.E., M.L., C.Y., M.C., X.L., L.M.-S., A.O.A., J.S.Y., P.N.B., P.D., and J.L. performed research; J.X., Y.Z., L.M.-S., J.S.Y., M.E.P., S.-L.L., P.D., and J.L. contributed new reagents/analytic tools; J.X., Y.Z., P.Q., M.M.S., S.J.Y., J.M., I.T., J.M.H., J.P.E., M.L., X.L., P.N.B., M.E.P., S.-L.L., P.D., and J.L. analyzed data; and J.X., Y.Z., and J.L. wrote the paper.

1. Q. Li *et al.*, Early transmission dynamics in Wuhan, China, of novel coronavirus-infected pneumonia. *N. Engl. J. Med.* **382**, 1199–1207 (2020).
2. N. Zhu *et al.*, A novel coronavirus from patients with pneumonia in China, 2019. *N. Engl. J. Med.* **382**, 727–733 (2020).
3. F. Krammer, SARS-CoV-2 vaccines in development. *Nature* **586**, 516–527 (2020).
4. L. R. Baden *et al.*, Efficacy and safety of the mRNA-1273 SARS-CoV-2 vaccine. *N. Engl. J. Med.* **384**, 403–416 (2021).
5. F. P. Polack *et al.*, Safety and efficacy of the BNT162b2 mRNA Covid-19 vaccine. *N. Engl. J. Med.* **383**, 2603–2615 (2020).
6. J. Sadoff *et al.*, Safety and efficacy of single-dose Ad26.COV2.S vaccine against Covid-19. *N. Engl. J. Med.* **384**, 2187–2201 (2021).
7. Y. L. Cao *et al.*, BA.2.12.1, BA.4 and BA.5 escape antibodies elicited by Omicron infection. *Nature* **608**, 593–602 (2022).
8. C. Liu *et al.*, Reduced neutralization of SARS-CoV-2 B.1.617 by vaccine and convalescent serum. *Cell* **184**, 4220–4236.e13 (2021).
9. N. Wolter *et al.*, Early assessment of the clinical severity of the SARS-CoV-2 omicron variant in South Africa: A data linkage study. *Lancet* **399**, 437–446 (2022).
10. W. Dejnirattisai *et al.*, SARS-CoV-2 Omicron-B.1.1.529 leads to widespread escape from neutralizing antibody responses. *Cell* **185**, 467–484.e15 (2022).
11. J. S. Tregoning, K. E. Flight, S. L. Higham, Z. Y. Wang, B. E. Pierce, Progress of the COVID-19 vaccine effort: Viruses, vaccines and variants versus efficacy, effectiveness and escape. *Nat. Rev. Immunol.* **21**, 626–636 (2021).
12. C. Fenwick *et al.*, A high-throughput cell– and virus-free assay shows reduced neutralization of SARS-CoV-2 variants by COVID-19 convalescent plasma. *Sci. Transl. Med.* **13**, eabi8452 (2021).
13. F. Kauffmann *et al.*, Measles, mumps, rubella prevention: How can we do better? *Expert Rev. Vaccines* **20**, 811–826 (2021).
14. W. H. W. Lin *et al.*, A durable protective immune response to wild-type measles virus infection of macaques is due to viral replication and spread in lymphoid tissues. *Sci. Transl. Med.* **12**, eaax7799 (2020).
15. F. Tangy, H. Y. Naim, Live attenuated measles vaccine as a potential multivalent pediatric vaccination vector. *Viral Immunol.* **18**, 317–326 (2005).
16. M. Liniger *et al.*, Induction of neutralising antibodies and cellular immune responses against SARS coronavirus by recombinant measles viruses. *Vaccine* **26**, 2164–2174 (2008).
17. M. J. Lu *et al.*, A safe and highly efficacious measles virus-based vaccine expressing SARS-CoV-2 stabilized prefusion spike. *Proc. Natl. Acad. Sci. U.S.A.* **118**, e2026153118 (2021).
18. Y. Zhang *et al.*, A highly efficacious live attenuated mumps virus-based SARS-CoV-2 vaccine candidate expressing a six-proline stabilized prefusion spike. *Proc. Natl. Acad. Sci. U.S.A.* **119**, e2201616119 (2022).
19. G. Amexis *et al.*, Sequence diversity of Jeryl Lynn strain of mumps virus: Quantitative mutant analysis for vaccine quality control. *Virology* **300**, 171–179 (2002).
20. C. L. Hsieh *et al.*, Structure-based design of prefusion-stabilized SARS-CoV-2 spikes. *Science* **369**, 1501–1505 (2020).
21. D. Wrapp *et al.*, Cryo-EM structure of the 2019-nCoV spike in the prefusion conformation. *Science* **367**, 1260–1263 (2020).
22. Y. Zhang *et al.*, Recombinant measles virus expressing prefusion spike protein stabilized by six rather than two prolines is more efficacious against SARS-CoV-2 infection. *J. Med. Virol.* **95**, e28687 (2023), 10.1002/jmv.28687.
23. C. Zeng *et al.*, Neutralizing antibody against SARS-CoV-2 spike in COVID-19 patients, health care workers, and convalescent plasma donors. *JCI Insight* **5**, e143213 (2020).
24. J. Grau-Exposito *et al.*, Peripheral and lung resident memory T cell responses against SARS-CoV-2. *Nat. Commun.* **12**, 3010 (2021).
25. A. Flemming, Cross-reactive tissue-resident CD8(+) T cells may provide first line of defence against SARS-CoV-2. *Nat. Rev. Immunol.* **21**, 693 (2021).
26. J. Tang *et al.*, Respiratory mucosal immunity against SARS-CoV-2 after mRNA vaccination. *Sci. Immunol.* **7**, eadd4853 (2022).
27. R. L. Murphy *et al.*, The need for more holistic immune profiling in next-generation SARS-CoV-2 vaccine trials. *Front. Immunol.* **13**, 923106 (2022).
28. A. Iwasaki, Exploiting mucosal immunity for antiviral vaccines. *Annu. Rev. Immunol.* **34**, 575–608 (2016).
29. N. Low *et al.*, A randomized, controlled trial of an aerosolized vaccine against measles. *N. Engl. J. Med.* **372**, 1519–1529 (2015).
30. N. Low, S. Kraemer, M. Schneider, A. M. H. Restrepo, Immunogenicity and safety of aerosolized measles vaccine: Systematic review and meta-analysis. *Vaccine* **26**, 383–398 (2008).
31. V. P. Krasnova, N. V. Iuminova, V. A. Liashenko, An intranasal method of revaccination against mumps. *Vopr. Virusol.* **39**, 24–26 (1994).
32. N. V. Iuminova, V. P. Krasnova, V. A. Liashenko, The specific activity and immunological safety of a live mumps vaccine from the Leningrad-3 strain in intranasally revaccinated adult subjects. *Vopr. Virusol.* **39**, 113–116 (1994).
33. S. A. Rubin, M. A. Afzal, Neurovirulence safety testing of mumps vaccines–Historical perspective and current status. *Vaccine* **29**, 2850–2855 (2011).
34. M. Lu *et al.*, SARS-CoV-2 prefusion spike protein stabilized by six rather than two prolines is more potent for inducing antibodies that neutralize viral variants of concern. *Proc. Natl. Acad. Sci. U. S. A.* **119**, e2110105119 (2022).
35. F. Vanhoutte *et al.*, Safety and immunogenicity of the measles vector-based SARS-CoV-2 vaccine candidate, V591, in adults: results from a phase 1/2 randomised, double-blind, placebo-controlled, dose-ranging trial. *Ebiomedicine* **75**, 103811 (2022).
36. O. Launay *et al.*, Safety and immunogenicity of a measles-vectored SARS-CoV-2 vaccine candidate, V591/TMV-083, in healthy adults: Results of a randomized, placebo-controlled Phase I study. *EBioMedicine* **75**, 103810 (2022).
37. P. N. Frantz *et al.*, A live measles-vectored COVID-19 vaccine induces strong immunity and protection from SARS-CoV-2 challenge in mice and hamsters. *Nat. Commun.* **12**, 6277 (2021).
38. M. C. Knuchel *et al.*, Relevance of a pre-existing measles immunity prior immunization with a recombinant measles virus vector. *Hum. Vaccin. Immunother.* **9**, 599–606 (2013).
39. A. Ebenig, M. V. Lange, M. D. Muhlebach, Versatility of live-attenuated measles viruses as platform technology for recombinant vaccines. *NPJ Vaccines* **7**, 119 (2022).
40. M. Mateo *et al.*, Rapid protection induced by a single-shot Lassa vaccine in male cynomolgus monkeys. *Nat. Commun.* **14**, 1352 (2023).
41. E. C. Reisinger *et al.*, Immunogenicity, safety, and tolerability of the measles-vectored chikungunya virus vaccine MV-CHIK: A double-blind, randomised, placebo-controlled and active-controlled phase 2 trial. *Lancet* **392**, 2718–2727 (2019).